Identifying fault activation during hydraulic stimulation in the Barnett shale: source mechanisms, *b* values, and energy release analyses of microseismicity

Scott Wessels, Michael Kratz, Alejandro De La Pena, MicroSeismic Inc.*

Summary

Identification of fault planes that intersect horizontal wellbores is critical to optimizing formation stimulation, preventing waste of valuable time and materials, and avoiding the establishment of fluid flow pathways into non-target formations, such as aquifers. We can detect and locate microseismic events accurately over a broad area using a large near surface seismic monitoring array. In addition, source mechanism inversion techniques can be used to determine the method of failure experienced by the rock formation, expanding our understanding of the dynamics involved in hydraulic fracturing. Events in this analysis are segregated into two populations based upon the distinct source mechanisms present. Spatial and temporal analysis of frequency magnitude distributions (FMD) allows us to characterize trends useful in assessing the hydraulic treatment efficiency. This information can assist in interpretation of faults in a 3D seismic volume to delineate faults in reservoirs, or when used alone, identify faults of subseismic displacement to further optimize future well placement. Also *b* values and source mechanisms can help to better define stimulated reservoir volumes (SRV) by indicating the effective level of stimulation.

Introduction

Microseismic monitoring of hydraulic fracture stimulation in low permeability reservoirs has grown to be a critical source of information for operators working to optimize well treatment plans. Information obtained from microseismic monitoring provides us with a better understanding of rock mechanics within the reservoir. One aspect of utmost importance is identifying pre-existing tectonic faults that have the capacity to capture one or more stages of valuable frac fluids and proppant without adding significantly to the productivity of the well, or possibly harming productivity by accessing a nearby aquifer.

Source mechanism inversion of microseismic events can be used to identify different failure mechanisms induced by fluid pressure in the reservoir. By comparing the energy distributions of event populations segregated by source mechanism and integrating other information, such as spatial and temporal distribution of events, we begin to see clear differences between these populations that can be used to further identify what type of activity is taking place within the reservoir. By examining the FMD of event populations we can also determine if a particular type of mechanism is associated with fault activity or reactivation of natural fractures (De La Pena et al., 2011).

In this study we examine the observed microseismicity associated with four horizontal wells completed in the Barnett Shale Formation in the Ft. Worth Basin, Midcontinent USA (Figure 1). The well horizontals are oriented perpendicular to maximum horizontal stress (Heidbach et al., 2009).

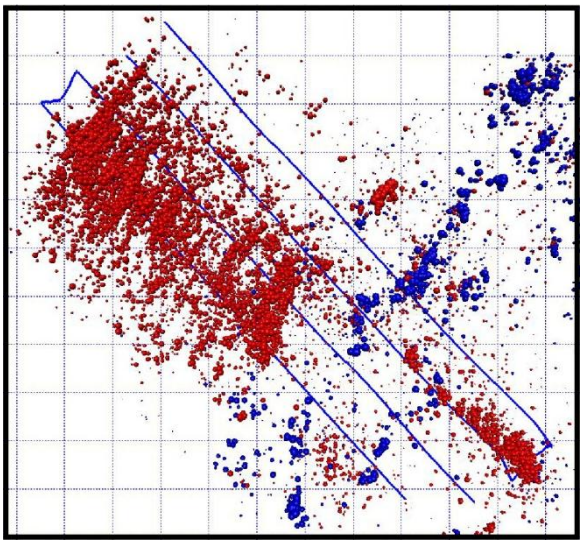

Figure 1. Map of wellbores and microseismic events colored by mechanism and sized by magnitude. Events interpreted to be related to natural fracture stimulation are in red, while fault related events are shown in blue. There are a total of 12,094 events shown here, of which 86% are natural fracture events. Grid squares are 500 ft by 500 ft.

Methodology

The dataset used for this study was acquired using BuriedArray™ technology and microseismic events were located using Passive Seismic Emission Tomography (PSET®). Two different source mechanisms were identified by inversion of several individual events following the same method explained by Williams-Stroud et al. (2010). The failure mechanisms are used to differentiate between events generated by reactivation of natural fractures and events generated by stimulation of a pre-existing fault plane intersecting the wellbore (De La Pena et al., 2011), herein referred to as fracture and fault events, respectively.

We used Zmap software (Weimer, 2001) to analyze spatial variation of *b* values over the areal extent of the microseismic volume. Grid cells are set at 0.001 degrees latitude and longitude. The magnitude of completeness, M_c, which is the lowest magnitude at which all events of that size are detected, was calculated using the maximum curvature method and *b* values were calculated using the maximum likelihood method (Woessner and Weimer, 2005). Frequency magnitude distributions are determined by plotting moment magnitude bins of 0.1 against the log of the bin count. The *b* value was determined by measuring the slope of the histogram for magnitudes above a common M_c of -1.6 for consistency.

Cumulative energy release plots for each mechanism were created by first converting moment magnitude into Joules released per event using the following formula:

$$\log \mathbf{J} = 1.5M_w + 4.8$$

This formula is derived from the equation used by Kanamori and Anderson (1975) to convert moment magnitude to ergs and follows the Gutenberg-Richter energy relationship (Gutenberg and Richter, 1956). Cumulative energy released for a 24 hour period was then summed and normalized to 1 for each population to correct for the disparity in event count and total energy released by events of each mechanism. Slopes were then calculated within chosen time intervals to illustrate the variability in energy release rates of each mechanism.

Statistical Analysis

Examining the FMD of events can give us more information about how the rock formation breaks and what external factors may be involved. Maxwell et al. (2009) and Downie et al. (2010) differentiate fault movement from fracture stimulation by comparing the slope (*b* value) on FMD plots for different populations of events. Figure 2 shows two different *b* value populations—slopes of ~2 for fracture events and ~1 for fault events (De La Pena et al., 2011). Schorlemmer et al. (2005) and Gulia et al. (2010) show empirically that *b* values vary systematically with the type of fault motion, such that the *b* value of a normal fault will be greater than that of a strike-slip fault, and a strike-slip fault will have a greater *b* value than a thrust fault. Because thrust faults occur in higher stress regimes than normal faults, it was inferred that *b* values can be used as a stress state indicator that is inversely related to the stress regime.

Fault events on average release a greater amount of energy and have a greater maximum magnitude when compared to fracture events; however, there are significantly fewer fault events than fracture events within this dataset. This is a result of the relatively small but linear area affected by the fault relative to the broad and well distributed fracture development.

The spatial variation in *b* values (Figure 3) indicates the relative presence of fault activity vs. fracture activity, and largely mirrors the event distribution seen in Figure 1. Lower *b* values are concentrated where the fault crosses the wellbores whereas higher *b* values indicate typical fracture event generation. The spatial distribution of *b* values in Figure 3 show the variation between areas of effectively stimulated reservoir relative to areas that may not have been so effectively stimulated. The highest *b* values located near the outer edges of the treated area are anomalously high due to an insufficient event population per cell. FMD plots for individual cells (Figure 4) within Figure 3 are in agreement with our *b* values for the total population of fault and fracture events.

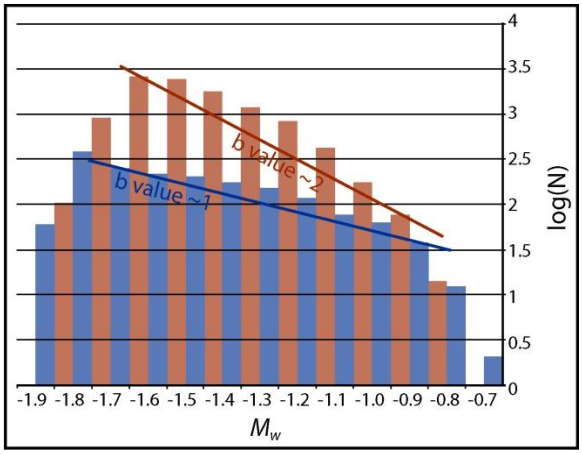

Figure 2. A non-cumulative FMD histogram of fault (blue) and fracture events (red) shows the log of the number of events (y-axis) per 0.1 magnitude bin (x-axis). The *b* value of the fracture events is ~2 whereas the *b* value for fault events is ~1.

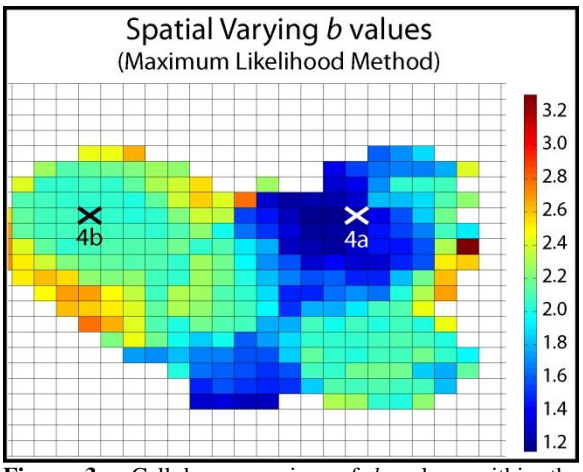

Figure 3. Cellular map view of *b* values within the treatment area. Lower values are associated with fault activity whereas higher *b* values are indicative of more natural fracture event generation. The highest values on the outer edges are due to insufficient event populations for FMD calculations. The location individual cells used for Figures 4a and 4b are indicated.

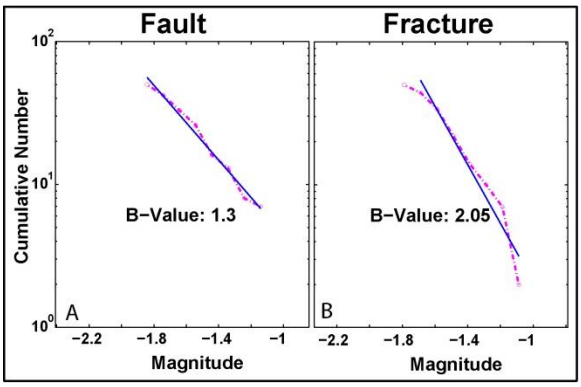

Figure 4. Cumulative FMD plots for individual cells in Figure 3. A) A *b* value of 1.3 indicates fault related activity. B) A higher *b* value of 2.05 suggests a lower local strain rate and therefore a typical fracture failure mechanism.

Timing and Rates of Energy Release

Microseismicity generated by hydraulic pumping within a formation with low differential stress should theoretically be coincident with the time of pumping, i.e. when fluid and proppant are forcibly added to the formation. Similarly, we would expect high stress areas of the formation to generate microseismicity during pumping and also between pumping intervals when accumulated stress is released. Using microseismic events generated during one 24 hour period (Figure 5), we show that fracture generated microseismicity is largely isolated to a restricted period of pumping time whereas fault events are distributed over a much longer period of time (Figure 6).

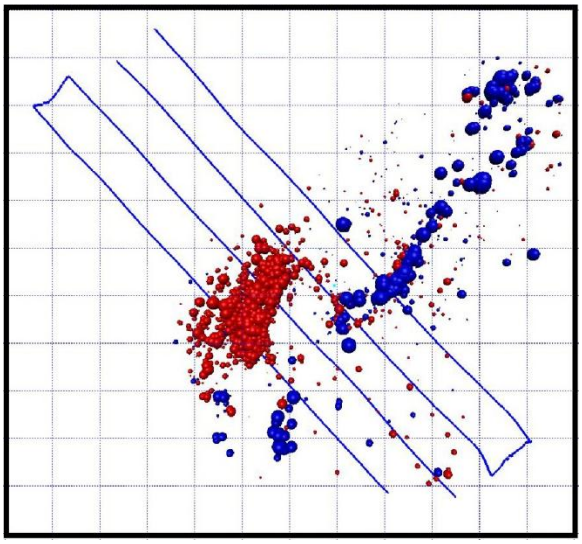

Figure 5. Map view of events used for time energy release comparison. All events shown occurred within a single 24 hour time period, which includes one fault affected stage (blue) and two fracture dominated stages (red).

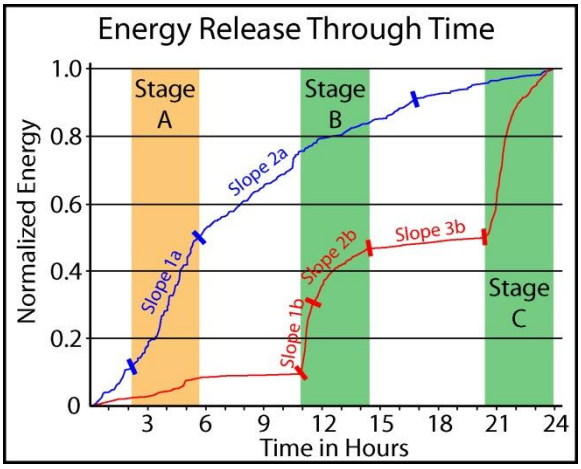

Figure 6. Normalized cumulative energy release for a 24 hour time period, separated by mechanism. Three complete hydraulic fracture stages took place during this time. Stage A has significant fault interaction while stage B and C generate very little fault related microseismicity.

Looking at Table 1 and Figure 6, fault energy release during pumping occurs at a moderate rate (slope 1a) followed by a lower rate (slope 2a) that approximates an exponential decline curve. In contrast, we see that hydraulically stimulated natural fractures release microseismic energy at a very high rate initially (slope 1b),

followed by a lesser energy release rate (slope 2b) and near inactivity between stages (slope 3b).

Table 1. Slope Values

Failure Type	Slope	Slope Value (J/s)
Fault	1a	9.0
	2a	3.0
Fracture	1b	42.2
	2b	7.8
	3b	0.8

Therefore we find that microseismic energy released by reactivated fractures is cyclical, predictable, and directly controlled by pumping (slopes 1b, 2b). Between pumping some fracture microseismicity is present, likely due to metastable energy release as the local stress state moves toward equilibrium. The energy release rate of the fault slope 1a is much less than that of the fracture slope 1b, both of which are generated during pumping. The large difference is likely because the fault zone can accept a larger volume of fluids per Joule of microseismic energy released per unit of time. Slope 2a represents the gradual release of energy along the fault plane, which continues for the remainder of the 24 hour time period. Over the continuing course of the stimulation, total energy released in fault affected stages is reduced relative to fracture only stages.

Conclusions

The use of source mechanism inversion to differentiate between rock failure mechanisms combined with *b* value analysis and energy release rates can give insight into the local stress of the reservoir and confirm or deny the presence of stressed tectonic faults. The type of mechanism that is most mechanically dependent upon pumping can be assumed to be the desired fracture type because it is related to events that are evenly distributed throughout the reservoir rather than being related to large fault-like features. If there is a mechanism that exhibits energy release rates that are not dependent upon the pumping schedule it is likely to be a pre-existing feature that is optimally oriented to fail in the current stress field. These assumptions are validated by *b* value analysis of the event populations and spatial trends of the microseismic events. Spatial *b* value distribution maps are a potentially powerful tool to better estimate what portions of the reservoir are successfully stimulated.

This information can be used to better define stimulated reservoir volumes by separating mechanically independent (fault related) microseismicity from the total interpreted stimulated volume to more accurately represent the volume of rock that fractured under desired conditions. The presence of relatively large magnitude events after the fracture stage is completed can also indicate stimulation of a fault plane. If this data is available to an operator during hydraulic stimulation it can indicate whether a fault is stimulated, allowing the operator to make a decision to alter the pumping schedule or continue treatment on an interval away from the fault plane, thereby optimizing costs, use of materials, time, and treatment efficiency.

Acknowledgments

Thank you to Sherilyn Williams-Stroud, Rongmao Zhou, Kenny Lew, and Christine Remington for many insightful comments. Thank you to Alan Gunnell and Jude Numa for their assistance processing and analyzing this dataset. Most of all, thank you to MicroSeismic, Inc. for providing the data, resources, expertise and support required to complete this analysis.

EDITED REFERENCES

Note: This reference list is a copy-edited version of the reference list submitted by the author. Reference lists for the 2011 SEG Technical Program Expanded Abstracts have been copy edited so that references provided with the online metadata for each paper will achieve a high degree of linking to cited sources that appear on the Web.

REFERENCES

De La Pena, A., S. A. Wessels, A. R. Gunnell, K. J. Numa, S. Williams-Stroud, L. Eisner, M. Thornton, and M. Mueller, 2011, Fault or frac? Source mechanism and b value detection of fault fracturing — A Barnett case study: Presented at the 73rd Annual International Conference and Exhibition, EAGE.

Downie, R. C., E. Kronenberger, and S. C. Maxwell, 2010, Using microseismic source parameters to evaluate the influence of faults on fracture treatments — A geophysical approach to interpretation: SPE.

Gulia, L., S. Wiemer, and D. Schorlemmer, 2010, Asperity-based earthquake likelihood models for Italy: Annals of Geophysics, **53**, no. 3, 63–75.

Gutenberg, B., and C. F. Richter, 1956, Magnitude and energy of earthquakes: Annali di Geofisica, **9**, 1–15.

Heidbach, O., M. Tingay, A. Barth, J. Reinecker, D. Kurfeß, and B. Müller, 2009, The world stress map based on the database release 2008, equatorial scale 1:46,000,000: Commission for the Geological Map of the World, Paris, doi:10.1594/GFZ.WSM.Map2009.

Kanamori, H., and D. L. Anderson, 1975, Theoretical basis of some empirical relations in seismology: Bulletin of the Seismological Society of America, **65**, 1073–1096.

Maxwell, S. C., M. Jones, R. Parker, S. Miong, S. Leaney, D. Dorval, D. D'Amico, J. Logel, E. Anderson, and K. Hammermaster, 2009, Fault activation during hydraulic fracturing: 79th Annual International Meeting, SEG, Expanded Abstracts, **28**, 1552.

Schorlemmer, D., S. Wiemer, and M. Wyss, 2005, Variations in earthquake-size distribution across different stress regimes: Nature, **437**, no. 7058, 539–542, doi:10.1038/nature04094.

Wiemer, S., 2001, A software package to analyze seismicity: ZMAP: Seismological Research Letters, **72**, no. 3, 373–383, doi:10.1785/gssrl.72.3.373.

Woessner, J., and S. Weimer, 2005, Assessing the quality of earthquake catalogs: Estimating the magnitude of completeness and its uncertainty: Bulletin of the Seismological Society of America, **95**, no. 2, 684–698, doi:10.1785/0120040007.